Tremendous tunneling magnetoresistance effects based on van der Waals room-temperature ferromagnet Fe₃GaTe₂ with highly spin-polarized Fermi surfaces

Xinlu Li[1#], Meng Zhu[1#], Yaoyuan Wang[2], Fanxing Zheng[1], Jianting Dong[1], Ye Zhou[1], Long You [2], and Jia Zhang[1]*

¹School of Physics and Wuhan National High Magnetic Field Center,

Huazhong University of Science and Technology, 430074 Wuhan, China`

²School of Optical and Electronic Information,

Huazhong University of Science and Technology, 430074 Wuhan, China

* jiazhang@hust.edu.cn;

[#]These authors contributed equally to this work.

Abstract:

Recently, van der Waals (vdW) magnetic heterostructures have received increasing research attention in spintronics. However, the lack of room-temperature magnetic order of vdW material has largely impedes its development in practical spintronics devices. Inspired by the recently discovered vdW ferromagnet Fe₃GaTe₂, which has been shown to have magnetic order above room temperature and sizable perpendicular magnetic anisotropy, we investigate the basic electronic structure and magnetic properties of Fe₃GaTe₂ as well as tunneling magnetoresistance effect in magnetic tunnel junctions (MTJs) with structure of Fe₃GaTe₂/Insulator/Fe₃GaTe₂ by using first-principles calculations. It is found that Fe₃GaTe₂ with highly spin-polarized Fermi surface ensures that such magnetic tunnel junctions may have prominent tunneling magnetoresistance effect at room temperature even comparable to existing conventional AlOₓ and MgO-based MTJs. Our results suggest that Fe₃GaTe₂-based MTJs may be the promising candidate for realizing long-waiting full magnetic vdW spintronic devices.

Keywords: vdW ferromagnet, magnetic tunnel junctions, spin-dependent transport, Fe₃GaTe₂, tunneling magnetoresistance.

I. Introduction

Since the discovery of long-range magnetic order down to the monolayer limit in $Cr_2Ge_2Te_6$on page 11[1] and

CrI_3[2] materials in 2017, a wide variety of emerging two-dimensional (2D) magnetic materials have been

discovered[3-6], which provide an effective materials platform for exploring novel 2D spintronics devices.

Since then, great progress has been made both in theoretical and experimental studies on van der Waals

(vdW) magnetic materials and related heterojunctions[7,8]. In particular, vdW heterojunctions with large

magnetoresistance have shown potential applications in spintronics devices such as magnetic random-

access memories and high-density hard disk drives.

For instance, CrI_3 has been used as a spin-filter barrier in graphite/CrI_3/graphite magnetic tunnel

junctions (MTJs)[9,10], nevertheless, a large continuous magnetic field and extremely low temperature is

required to maintain its magnetoresistance effect. Over the past few years, 2D magnetic heterojunctions

using Fe_3GeTe_2 as ferromagnetic electrodes have been widely reported[11-17]. It has been demonstrated that

tunneling magnetoresistance of 160% (at 4.2 K), 41% (at 10 K) and 300% (at 4.2 K) can be

experimentally achieved in all vdW heterostructure Fe_3GeTe_2/h-BN/Fe_3GeTe_2[14],

Fe_3GeTe_2/InSe/Fe_3GeTe_2[16] and Fe_3GeTe_2/h-BN/Fe_3GeTe_2[17], respectively. However, as the transition

temperature of bulk Fe_3GeTe_2 (220 K)[4] are still below room temperature (300 K), a much lower operating

temperature (< 10 K) is needed to achieve sizable TMR, which greatly hinders the practical applications

of magnetic vdW heterostructures. As a result, it is crucial to search vdW heterostructures with both high

transition temperatures and large TMR effect.

Recently, vdW ferromagnet Fe_3GaTe_2[18] with large perpendicular magnetocrystalline anisotropy

(MCA) energy density (~$4.79 \times 10^5 J/m^3$ at 300 K) and Curie temperature T_C (350–380 K) well above

room temperature has been discovered. Driven by this exciting finding, in this letter, we first examine

the basic magnetic properties of Fe_3GaTe_2 and then investigate the spin-dependent electron transport in

vdW MTJs based on Fe_3GaTe_2. In this case, Fe_3GaTe_2 is used as the ferromagnetic electrode of the MTJs,

while for the spacer layer we have chosen insulator h-BN and semiconductor 2H-WSe_2. We demonstrate

that the existence of a prevalent ultra-high tunneling magnetoresistance (TMR) effects, which mainly

stem from the highly spin-polarized Fermi surfaces of Fe_3GaTe_2. Our findings may stimulate further

experimental work on the realization of full vdW MTJs at room temperature.

II. Calculation methods

By using Vienna ab initial Package (VASP)[19], we first examine either generalized gradient approximation (GGA-PBE)[20] or local density approximation (LDA)[21,22] exchange-correlation functions could better describe Fe_3GaTe_2 by comparing calculated magnetic properties to available experiments[18]. The calculated magnetic moment and magnetocrystalline anisotropy (MCA) energy are found to fit better with experimental values[18] by using LDA functionals than GGA as shown in Table 1. LDA will then be employed in the following calculation for Fe_3GaTe_2 in the rest of this work. The details of the calculations can be found in the Supplementary Information S1.

Table 1. The calculated average magnetic moment per Fe atom and MCA energy of bulk Fe_3GaTe_2 by using GGA and LDA functionals in comparison with experimental values. Please note that the quantities calculated by first-principles should be considered at 0 K.

Magnetic properties of Fe_3GaTe_2	GGA	LDA	Experimental values[18]
M (μ_B/Fe)	1.93	1.76	1.68 (3 K) 1.18 (300 K)
MCA energy density ($*10^5$ J/m^3)	21.11	8.01	4.79 (300 K)

The remaining first-principles calculations of this work are performed by Quantum Espresso simulation package[23] using the projector augmented wave (PAW) method with Garrity-Bennett-Rabe-Vanderbilt (GRBV) 1.5 ultrasoft pseudopotentials[24]. The LDA of Perdew-Zunger (PZ)[21] is used for the exchange-correlation functional potentials. We use the $15 \times 15 \times 3$ Monkhorst-Pack k-points mesh for the self-consistent calculation, while the energy cutoff for plane-wave and charge density are set at 40 and 320 Ry, respectively.

For the magnetic tunnel junction (MTJ) based on Fe_3GaTe_2, the self-consistently calculations of scattering region are performed by using a k-point mesh of 15×15×1. And then, the electron transmissions of the MTJs are obtained by using the wave-function scattering method[25], matching the wave function between the left and right Fe_3GaTe_2 electrodes and the scattering region of the MTJs. The $k_{//}=(k_x, k_y)$-resolved electron transmissions is then calculated with the 200×200 $k_{//}$ mesh in the 2D Brillouin zone (2DBZ). The spin-dependent ballistic conductance of the MTJs is calculated by summarizing transmission over entire 2DBZ based on the Landauer-Büttiker formula[26-28] as follow:

$$G_\sigma = \frac{e^2}{h} \sum_{k_{//}} T_\sigma(k_{//})$$

where $T_\sigma (k_{//})$ denotes the spin and $k_{//}$-resolved electron transmission, e is the elementary charge, and h is the Planck constant. The TMR ratio is defined as TMR = $(G_P - G_{AP})/G_{AP}$, where G_P and G_{AP} are the conductance for parallel (P) and antiparallel (AP) alignments of the magnetization orientations of two Fe_3GaTe_2 electrodes, respectively. The resistance-area product (RA) is another important physical quantity which can be evaluated from the conductance[13].

III. Results and discussions

Basic electronic structure and magnetic properties of Fe_3GaTe_2

The atomic structure of Fe_3GaTe_2 is the same as well studied Fe_3GeTe_2, which has a layered hexagonal crystal structure with a space group $P6_3$/mmc (No. 194). The atomic structure of bulk Fe_3GaTe_2 is depicted in Fig. 1a, which illustrates the AB-stacking of Fe_3GaTe_2 with two-layer periodicity along the c-axis, separated by vdW gap. In each monolayer, the Fe atoms are located in two inequivalent Wyckoff sites Fe^I and Fe^{II} with different magnetic moments. The monolayer comprises five atomic layers with the central layer forming a Fe^{II}-Ga honeycomb lattice, then the next two layers form vertical Fe^I dumbbells, while the top and bottom layers are occupied by Te sandwiching the Fe_3Ga layers. The calculated spin-dependent band structure and density of states (DOS) of Fe_3GaTe_2 are shown in Fig. 1c and 1d. A large spin-polarization at the Fermi level can be observed from the band structure and DOS. From the LDA self-consistent calculations, the average magnetic moment of bulk Fe_3GaTe_2 is found to be 1.76 μ_B/Fe, which agree well with the experimental value of 1.68 μ_B/Fe[18] at 3 K as shown in Table 1.
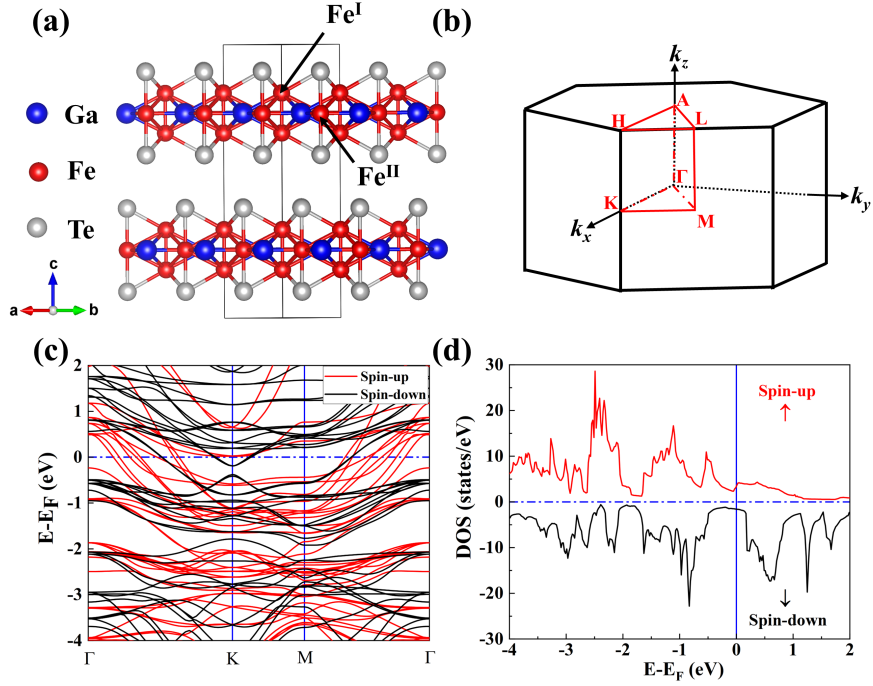
Fig. 1. (a) The crystal structure of bulk Fe₃GaTe₂, where the solid black box indicates the primitive cell of bulk Fe₃GaTe₂. (b) Brillouin zone and high-symmetry k path of a hexagonal lattice. (c) and (d) are the spin-polarized band structures and density of states for bulk Fe₃GaTe₂, respectively.

In the next, we first extract magnetic interaction parameters of Fe₃GaTe₂ and then perform Monte Carlo simulation to evaluate its Curie temperature. The spin Hamiltonian of Fe₃GaTe₂ can be modeled as follows:

$$H = -\sum_{i \neq j} J_{ij} S_i \cdot S_j - K \sum_i S_{i,z}^2$$

Where J_{ij} is the Heisenberg exchange interaction between spin moment at site i and j, S_i is a unit vector pointing to the local spin moment, K is the uniaxial magnetic anisotropy constant. The interatomic Heisenberg exchange interactions have been calculated by using SPR-KKR package based on KKR-Green's function method using Lichtenstein's formula[29]. The calculated exchange interaction energy J_{ij} for the first six nearest neighbors are listed in Table 2. Due to the large ferromagnetic exchange interaction for the first two nearest neighbors (J₁=57.18 meV, J₂=17.03 meV), Fe₃GaTe₂ is supposed to be ferromagnetic with high Curie temperature. The magnetic easy-axis has been determined by comparing the energy of Fe₃GaTe₂ with spin axis pointing along various directions by considering spin-orbit coupling (SOC) in calculations. It turns out that Fe₃GaTe₂ shows magnetic easy axis along c-axis. The calculated MCA energy of bulk Fe₃GaTe₂ evaluated from the magnetic force theorem is found to be around 1.116 meV/u.c corresponding to 8.01×10⁵ J/m³ , which agrees with experimental magnetic

anisotropy energy (4.79×10^5 J/m^3 at 300 K).

Once the exchange interaction and magnetic anisotropy energy are extracted, the Curie temperature of Fe$_3$GaTe$_2$ is then determined by Monte Carlo simulations using UppASD package[30]. The Curie temperature T_C of bulk and monolayer Fe$_3$GaTe$_2$ can be obtained by fitting the normalized magnetization M/M_S by the following equation[31]

$$m(T) = \left(1 - \frac{T}{T_C}\right)^{\beta}$$

Where β is the critical magnetization exponent with a typical value of around 0.3. As shown in Fig. 1b, the Curie temperature of bulk Fe$_3$GaTe$_2$ is fitted to be around 406 K, which is close to the experimental T_C of 380 K[18]. The simulated Curie temperature of monolayer Fe$_3$GaTe$_2$ is 320 K, indicating that Fe$_3$GaTe$_2$ will remain ferromagnetic above room temperature even down to monolayer limit.
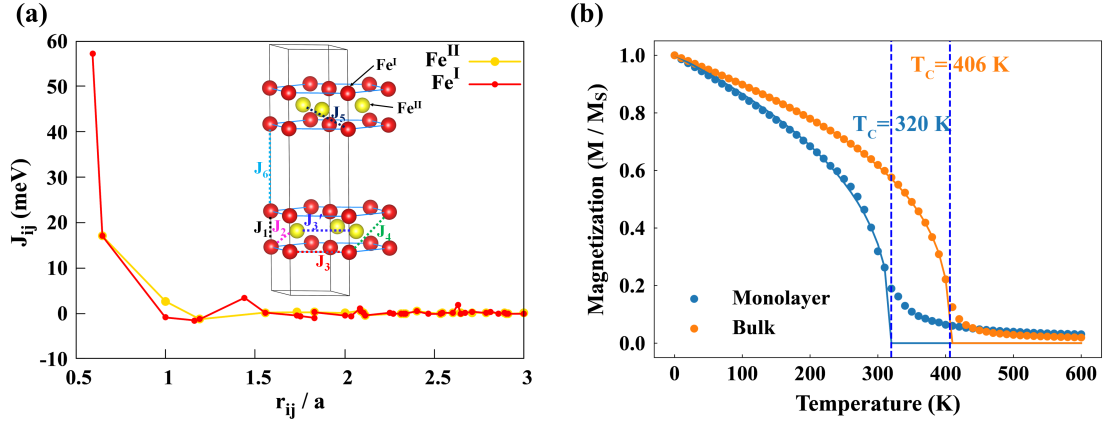

Fig. 2. (a)The calculated Heisenberg exchange interactions as a function of distance between pairs of Fe atoms by taking Fe^{I} (red line) and Fe^{II} (gold line) as center atoms in bulk Fe$_3$GaTe$_2$.The first six Fe-Fe exchange interaction path is indicated, where only the Fe atoms have been displayed in crystal structure. (b) The calculated normalized magnetization (depicted in solid circles) as a function of temperature for monolayer and bulk Fe$_3$GaTe$_2$ obtained from Monte Carlo simulation, where the solid lines are the fitted curve.

Table 2. The calculated Heisenberg exchange interaction J_N of bulk Fe$_3$GaTe$_2$ for the first 6 nearest neighbors, where Ns is the coordination number.

J_N	Distance (Å)	Type	Ns	J_{ij} (meV)
J_1	2.37	Fe^{I} - Fe^{I}	1	57.18
J_2	2.59	Fe^{I} - Fe^{II}	6	17.02
J_3	3.99	Fe^{I} - Fe^{I}	6	-0.92
J_3'	3.99	Fe^{II} - Fe^{II}	6	2.66
J_4	4.64	Fe^{I} - Fe^{I}	6	-1.55
J_5	4.75	Fe^{I} - Fe^{II}	6	-1.29
J_6	5.74	Fe^{I} - Fe^{I} (interlayer)	1	3.43

Tunneling magnetoresistance effect in the Fe₃GaTe₂-based vdW MTJs

In vdW magnetic tunnel junctions, spin-dependent transport and TMR at zero bias is mainly determined by the spin-polarization on Fermi surface of ferromagnetic electrode. Before investigating TMR effect in Fe₃GaTe₂-based vdW MTJs, we first calculate the Fermi surfaces of bulk Fe₃GaTe₂. Fig 3a and 3b show the spin-resolved three-dimensional (3D) Fermi surface of Fe₃GaTe₂ and Fig 3c and 3d illustrate its 2D Fermi surface projected onto 2DBZ. From the 2D Fermi surfaces, one can obtain the number of available Bloch states (conduction channels) of bulk Fe₃GaTe₂ at each $k_{//}=(k_x, k_y)$ points in the 2DBZ. It is clear that the 2D Fermi surface of spin down channel has few overlaps with spin up channel (Fig. 3e), which indicates highly spin-polarized Fermi surfaces, and should produce a large tunneling magnetoresistance effect in the vdW MTJs based on Fe₃GaTe₂.

For comparison, we also plot the 3D and 2D Fermi surfaces for other two well-studied vdW ferromagnets: Fe₃GeTe₂ ($T_C\sim220$ K)[4] and $1T$-CrTe₂ ($T_C\sim310$ K)[32]. It can be observed that Fe₃GeTe₂ (Fig. 3f-g) have conduction channels around the Gamma point for both spin channels. As a result, the spin polarization on Fermi surface of Fe₃GeTe₂ is lower than Fe₃GaTe₂. On the other hand, although CrTe₂ have relatively high Curie temperature above 300 K, its two spin conduction channels have been overlapped in a large portion of BZ (Fig 3k-o), which indicates a low spin-polarization on Fermi surfaces and much lower TMR by using CrTe₂ as electrodes in vdW MTJs.
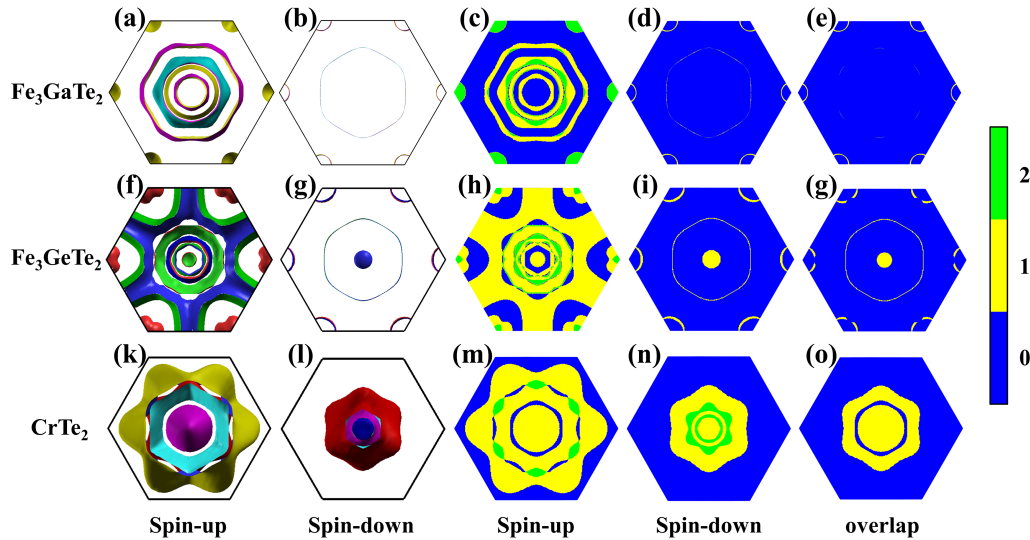

Fig. 3. (a) and (b) are the spin-up and spin-down 3D Fermi surfaces of bulk Fe₃GaTe₂, respectively, which are plotted using the xcrysden package[22]. (c) and (d) are the projected Fermi surfaces in the 2DBZ of bulk Fe₃GaTe₂. (e) shows the overlapped region for spin up and spin down channels. (f) - (g) and (k) - (o) show the corresponding 3D, 2D and overlapped Fermi surfaces for bulk Fe₃GeTe₂ and CrTe₂, respectively. The color bar at the right side of lower

panel indicates the number of available Bloch states at Fermi level.

Based on the above analysis, we build vdW MTJs comprised of Fe_3GaTe_2 electrodes and monolayer h-BN barrier, using the $\sqrt{3} \times \sqrt{3}$ in-plane unit cell of h-BN matched at the interface with the unit cell of Fe_3GaTe_2 electrode, as illustrated in Fig. 4a. The optimized vertical interlayer space between Fe_3GaTe_2 electrodes and h-BN barrier is 3.50 Å, which is a typical vdW interaction distance. We then calculate the tunneling conductance of the MTJs for parallel (Fig. 4b and 4c) and antiparallel (Fig. 4d) magnetization alignments of the left and right Fe_3GaTe_2 electrodes. The spin-up (Fig. 4b) and spin-down (Fig. 4c) electron transmission for parallel configuration are in accordance with the conduction channels of bulk Fe_3GaTe_2 shown in Fig. 3c and 3d. For antiparallel configuration, the electron transmission shown in Fig. 4d is consistent with the overlapped Fermi surface shown in Fig.3e and have been greatly suppressed owing to the mismatch of Fermi surfaces for two spin channels. In consequence, a tremendous TMR over 30000% has been achieved in Fe_3GaTe_2/h-BN$/Fe_3GaTe_2$ MTJ.

Without loss of generality, we also build another Fe_3GaTe_2-based MTJs by considering semiconductor 2H-WSe_2 and vacuum as tunnel barriers (Supporting Information Note 2). As listed in Table 3, Fe_3GaTe_2-based MTJs with both tunnel barriers all exhibit similarly large TMR (>10000%). It is worthy pointing out that such large TMR of Fe_3GaTe_2-based MTJs is around one order of magnitude larger than previously studied Fe_3GeTe_2-based MTJs[11]. Furthermore, we also compare the transport properties of Fe_3GaTe_2-based MTJs to another room temperature ferromagnet $CrTe_2$-based MTJs. By using insulator β-$MgCl_2$[33] (band-gap 5.42 eV) as tunnel barrier, the $CrTe_2/MgCl_2/CrTe_2$ MTJs are illustrated in Fig. 4b. As it can be seen from the spin-dependent transmission of $CrTe_2$-based MTJs shown in Fig. 4f-4h, the small mismatch between spin up and spin down conduction channels results in large transmission for antiparallel alignment in 2DBZ, which turns out to produce much smaller TMR of only around 25% (Table 3). These calculation results clearly indicate that Fe_3GaTe_2-based MTJs show great superiority over the existing vdW MTJs.
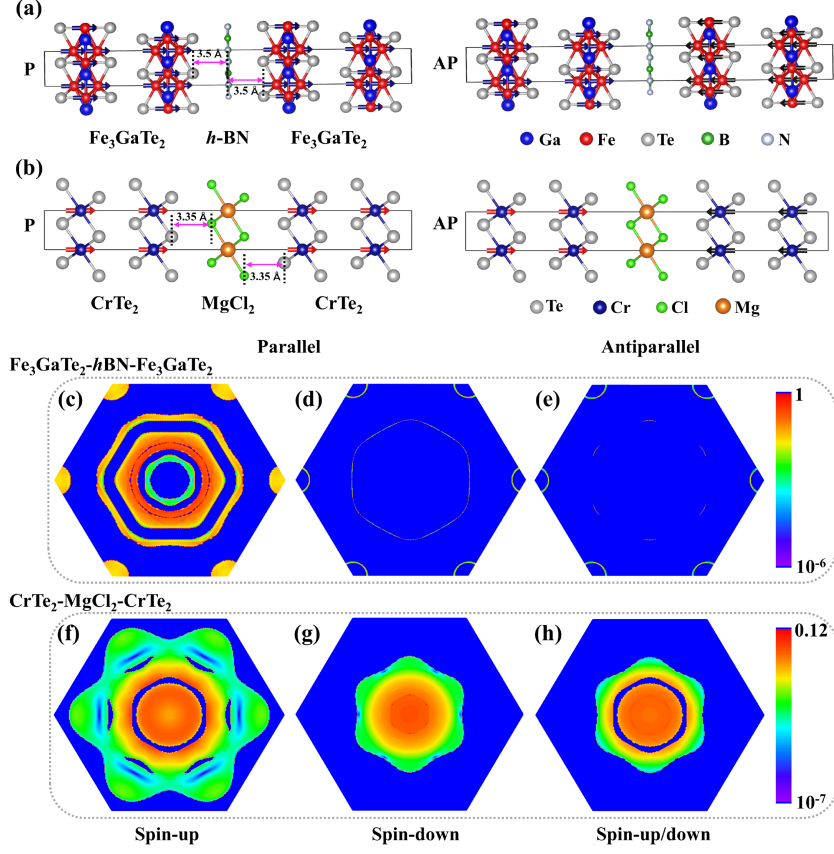
Fig. 4. Atomic structures of Fe_3GaTe_2/h-BN/Fe_3GaTe_2 (a) and $CrTe_2$/$MgCl_2$/$CrTe_2$ (b) MTJs with parallel (P) and antiparallel (AP) magnetization alignments of the two electrodes. Arrows on Fe and Cr atoms denote the direction of magnetic moments. (c) and (d) are the spin-up and spin-down $k_{//}$-resolved transmission distributions in 2DBZ of Fe_3GaTe_2/h-BN/Fe_3GaTe_2 in parallel configuration, respectively. (e) is the either-spin transmission for antiparallel state. (f)-(h) show the corresponding transmission of $CrTe_2$/$MgCl_2$/$CrTe_2$. Color scale alongside indicates the available transmission on a logarithmic scale.

Table 3. The spin-dependent transport properties of several different vdW MTJs when the magnetizations of two ferromagnetic electrodes are in P and AP alignments.

MTJ structures	Transmission of P state		Transmission of AP state		
	T	RA $(\Omega \times \mu m^2)$	T	RA $(\Omega \times \mu m^2)$	TMR (%)
Fe_3GaTe_2/h-BN/Fe_3GaTe_2	1.77×10^{-2}	**0.20**	5.49×10^{-5}	**64.66**	3.21×10^4
Fe_3GaTe_2/2H-WSe_2/Fe_3GaTe_2	9.79×10^{-2}	**0.11**	8.78×10^{-4}	**12.13**	1.11×10^4
Fe_3GaTe_2/vacuum/Fe_3GaTe_2	5.89×10^{-5}	**60.27**	2.81×10^{-8}	**1.26×10^5**	2.10×10^5
Fe_3GeTe_2/h-BN/Fe_3GeTe_2[11]	2.15×10^{-2}	**0.17**	3.38×10^{-4}	**10.53**	6.26×10^3
Fe_3GeTe_2/vacuum/Fe_3GeTe_2[11]	6.18×10^{-3}	**0.58**	4.44×10^{-5}	**80.16**	1.38×10^4
$CrTe_2$/$MgCl_2$/$CrTe_2$	3.81×10^{-3}	**0.84**	3.04×10^{-3}	**1.06**	25.12

The aforementioned transport investigations under zero bias of Fe_3GaTe_2-based MTJs are all conducted at Fermi energy (E_F). In reality, the Fermi level may shift away from E_F caused by doping, lattice strain, structural defections, *etc*. To further clarify the robust of large TMR in Fe_3GaTe_2-based MTJs, we investigate the energy dependence of Fermi surfaces for bulk Fe_3GaTe_2 within the energy range between E_F-0.15 eV and E_F+0.15 eV. As depicted in Fig. 5, in the studied energy range, the highly spin-polarized Fermi surfaces of Fe_3GaTe_2 have been preserved. Noteworthily, at E_F+0.1 eV and E_F+0.15 eV, the conduction channels between spin-up and spin-down are completely mismatched, corresponding to fully spin-polarized Fermi surfaces. By taking Fe_3GaTe_2/*h*-BN/Fe_3GaTe_2 MTJ as an example, as illustrated in Fig. 6, we explicitly calculate transmission and TMR as a function of energy. It turns out that for energy below E_F, the TMR ratios tend to first increase and then decrease as the energy decreases. Whereas for energy above E_F, the TMR ratios increase as the energies increases and reach infinity when energy is larger than 0.1 eV above E_F, due to the 100% spin-polarization of Fermi surfaces in 2DBZ. This result indicates that the Fe_3GaTe_2-based MTJ should have ultra-high TMR ratios in relatively wide energy window around Fermi energy.
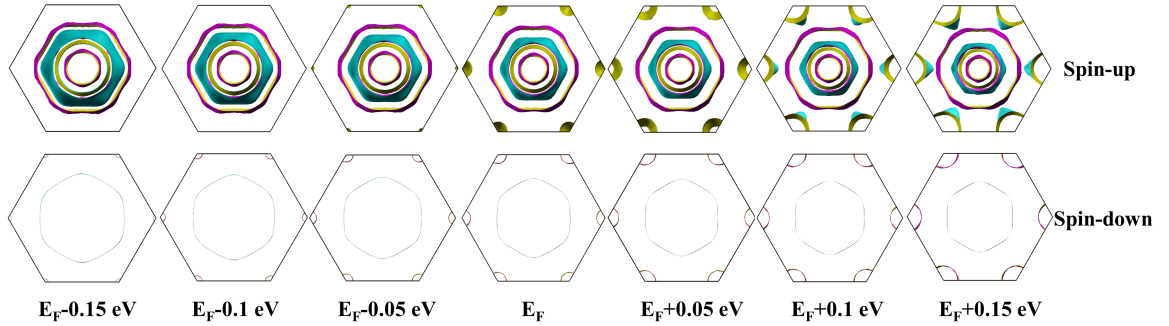

Fig. 5. The spin-up (upper panel) and spin-down (lower panel) Fermi surfaces of bulk Fe_3GaTe_2 around Fermi energy ranging from E_F-0.15 to E_F+0.15 eV.
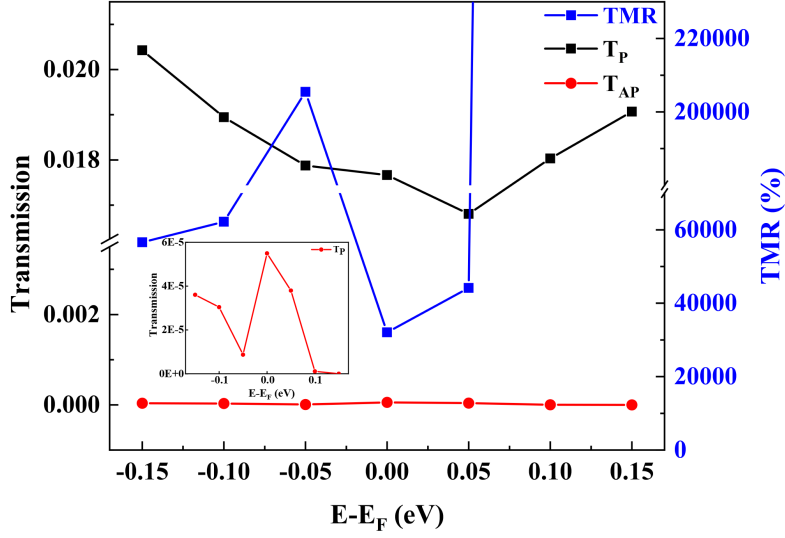
Fig. 6. The electron transmission for the parallel (T_P, in black) and antiparallel (T_{AP}, in red) states and the TMR (in blue, refer to right axis) as a function of energy in theFe₃GaTe₂/h-BN/Fe₃GaTe₂ MTJ. The electron transmission for the parallel (T_P, in black) and antiparallel (T_{AP}, in red) states and the TMR (in blue, refer to right axis) as a function of energy in theFe₃GaTe₂/h-BN/Fe₃GaTe₂ MTJ. The inset shows an enlarged view of transmission for antiparallel state as a function of energy.

IV. Summary and Conclusion

In summary, the spin-dependent transport properties in vdW MTJs based on ferromagnet Fe₃GaTe₂ have been investigated by first-principles calculations. Monte Carlo simulations have shown that the bulk Fe₃GaTe₂ have high Curie temperature above room temperature. The Fe₃GaTe₂-based vdW MTJs have an ultra-high TMR effect over 10000% originating from the highly spin-polarized Fermi surfaces. Moreover, the huge TMR effect is robust against the variation of Fermi energy. Our results indicate that Fe₃GaTe₂-based vdW MTJs are very promising for realizing remarkable room temperature TMR effect, which may be comparable or even larger than traditional CoFe/AlOₓ/CoFe and CoFeB/MgO/CoFeB MTJs. Our calculations provide a theoretical insight that may stimulate further experimental investigations on Fe₃GaTe₂-based magnetic vdW junctions towards high-performance room temperature spintronics devices.

ACKNOWLEDGMENTS

References:

1.   C. Gong, L. Li, Z. Li, H. Ji, A. Stern, Y. Xia, et al. Discovery of intrinsic ferromagnetism in two-dimensional van der Waals

crystals. Nature, 2017, 546(7657):265–269.

2. B. Huang, G. Clark, E. Navarro-Moratalla, D. R. Klein, R. Cheng, K. L. Seyler, et al. Layer-dependent ferromagnetism in a van der Waals crystal down to the monolayer limit. Nature, 2017, 546(7657):270–273.

3. K. S. Burch, D. Mandrus, J-G. Park. Magnetism in two-dimensional van der Waals materials. Nature, 2018, 563:47–52.

4. Y. Deng, Y. Yu, Y. Song, J. Zhang, N. Z. Wang, Z. Sun, et al. Gate-tunable room-temperature ferromagnetism in two-dimensional Fe_3GeTe_2. Nature, 2018, 563(7729):94–99.

5. A. F. May, C. A. Bridges, M. A. McGuire. Physical properties and thermal stability of $Fe_{5-x}GeTe_2$ single crystals. Phys. Rev. Materials, 2019, 3(10):104401.

6. J. Seo, D. Y. Kim, E. S. An, K. Kim, G.-Y. Kim, S.-Y. Hwang, et al. Nearly room temperature ferromagnetism in a magnetic metal-rich van der Waals metal. Sci. Adv., 2020, 6(3).

7. J. F. Dayen, S. J. Ray, O. Karis, I. J. Vera-Marun, M. V. Kamalakar. (2020). Two-dimensional van der Waals spinterfaces and magnetic-interfaces. Appl. Phys. Rev., 2020, 7(1), 011303.

8. E. Elahi, G. Dastgeer, P. R. Sharma, S. Nisar, M. Suleman, M. W. Iqbal, et al. A brief review on the spin valve magnetic tunnel junction composed of 2D materials. J. Phys. D: Appl. Phys., 2022, 55, 423001.

9. T. Song, X. Cai, M. W.-Y. Tu, X. Zhang, B. Huang, N. P. Wilson, et al. Giant tunneling magnetoresistance in spin-filter van der Waals heterostructures, Science 360, 1214 (2018).

10. D. R. Klein, D. MacNeill, J. L. Lado, D. Soriano, E. Navarro-Moratalla, K. Watanabe, et al. Probing magnetism in 2D van der Waals crystalline insulators via electron tunneling, Science 360, 1218 (2018).

11. X. Li, J.-T. Lü, J. Zhang, L. You, Y. Su, E. Y. Tsymbal. Spin-dependent transport in van der Waals magnetic tunnel junctions with Fe_3GeTe_2 electrodes. Nano Lett., 2019, 19(8):5133–5139.

12. Y. Su, X. Li, M. Zhu, J. Zhang, L. You, E. Y. Tsymbal. Van der Waals multiferroic tunnel junctions. Nano Lett., 2020, 21(1), 175-181.

13. X. Li, Y. Su, M. Zhu, F. Zheng, P. Zhang, J. Zhang, J.-T. Lü. Current-perpendicular-to-plane giant magnetoresistance effect in van der Waals heterostructures. Phys. Rev. Applied, 2021, 16(3), 034052.

14. Z. Wang, D. Sapkota, T. Taniguchi, K. Watanabe, D. Mandrus, A. F. Morpurgo. Tunneling spin valves based on Fe_3GeTe_2/hBN/Fe_3GeTe_2 van der Waals heterostructures. Nano Lett., 2018, 18(7):4303–4308.

15. H. Lin, F. Yan, C. Hu, Q. Lv, W. Zhu, Z. Wang, et al. Spin-valve effect in Fe_3GeTe_2/MoS_2/Fe_3GeTe_2 van der Waals heterostructures. ACS Appl. Mater. Interfaces, 2020, 12(39), 43921-43926.

16. W. Zhu, H. Lin, F. Yan, C. Hu, Z. Wang, L. Zhao, et al. Large tunneling magnetoresistance in van der Waals ferromagnet/semiconductor heterojunctions. Adv. Mater., 2021, 33(51), 2104658.

17. K. H. Min, D. H. Lee, S. J. Choi, I. H. Lee, J. Seo, D. W. Kim, et al. Tunable spin injection and detection across a van der Waals interface. Nat. Mater., 2022, 21(10), 1144-1149.

18. G. Zhang, F. Guo, H. Wu, X. Wen, L. Yang, W. Zhang, H. Chang. Above-room-temperature strong intrinsic ferromagnetism in 2D van der Waals Fe_3GaTe_2 with large perpendicular magnetic anisotropy. Nat. Commun., 2022, 13, 5067.

19. G. Kresse & J. Furthmüller, Efficiency of ab-initio total energy calculations for metals and semiconductors using a plane-wave basis set, Comput. Mater. Sci., 1996, 6, 15.

20. J. P. Perdew, K. Burke, M. Ernzerhof. Generalized gradient approximation made simple. Phys. Rev. Lett., 1996, 77(18):3865–3868.

21. J. P. Perdew, A. Zunger. Self-interaction correction to density-functional approximations for many-electron systems. Phys. Rev. B, 1981, 23(10), 5048.

22. D. M. Ceperley, B. J. Alder. Ground state of the electron gas by a stochastic method. Phys. Rev. Lett., 1980, 45(7), 566.

23. P. Giannozzi, et. al., Quantum Espresso: a modular and open-source software project for quantum simulations of materials, J. Phys.: Condens. Matter, 2009, 21, 395502.

24. K. F. Garrity, J. W. Bennett, K. M. Rabe, D. Vanderbilt, Pseudopotentials for high-throughput DFT calculations. Comput.

Mater. Sci., (2014), 81, 446-452.

25. A. Smogunov, A. D. Corso, E. Tosatti. Ballistic conductance of magnetic Co and Ni nanowires with ultrasoft pseudopotentials, Phys. Rev. B, 2004, 70, 045417.

26. R. Landauer, Spatial variation of currents and fields due to localized scatterers in metallic conduction, IBM J. Res. Dev. 1, 223 (1957).

27. R. Landauer, Electrical resistance of disordered one-dimensional lattices, Phil. Mag. 21, 863 (1970).

28. M. Büttiker, Y. Imry, R. Landauer, S. Pinhas, Generalized many-channel conductance formula with application to small rings, Phys. Rev. B 31, 6207 (1985).

29. H. Ebert, D. Koedderitzsch, J. Minar. Calculating condensed matter properties using the KKR-Green's function method—recent developments and applications. Rep. Prog. Phys., 2011, 74(9), 096501.

30. B. Skubic, J. Hellsvik, L. Nordström, O. Eriksson. A method for atomistic spin dynamics simulations: implementation and examples. J. Phys: condens. matter, 2008, 20(31), 315203.

31. R. F. L. Evans, W. J. Fan, P. Chureemart, T. A. Ostler, M. O. A. Ellis, R. W. Chantrell. Atomistic spin model simulations of magnetic nanomaterials. J. Phys: condens. Matter, 2014, 26, 103202.

32. H. Y. Lv, W. J. Lu, D. F. Shao, Y. Liu, Y. P. Sun. Strain-controlled switch between ferromagnetism and antiferromagnetism in $1T-\mathrm{Cr}X_2$ (X = Se, Te) monolayers. Phys. Rev. B, 2015, 92(21):214419.

33. F. Lu, W. Wang, X. Luo, X. Xie, Y. Chen, H. Dong, et al. A class of monolayer metal halogenides MX_2: Electronic structures and band alignments. Appl. Phys. Lett., 2016, 108(13): 132104.